SACLANTCEN MEMORANDUM
serial no.: SM-226

SACLANT UNDERSEA
RESEARCH CENTRE

MEMORANDUM

Analysis of basin backscattering in the Levantine Sea

J. Preston, T. Akal
and S. Fiori

December 1989

Page count for SM-226
(excluding covers)

Pages	Total
i–vi	6
1–28	28
	34

SACLANT Undersea Research Centre
Viale San Bartolomeo 400
19026 San Bartolomeo (SP), Italy

tel: 0187 540 111
telex: 271148 SACENT I

NORTH ATLANTIC TREATY ORGANIZATION

SACLANTCEN SM-226

Analysis of basin backscattering in the Levantine Sea

J. Preston, T. Akal and S. Fiori

The content of this document pertains to work performed under Project 05 of the SACLANTCEN Programme of Work. The document has been approved for release by The Director, SACLANTCEN.

Issued by:
Underwater Research Division

J.M. Hovem
Division Chief

intentionally blank page

Analysis of basin backscattering in the Levantine Sea

J. Preston, T. Akal and S. Fiori

Executive Summary: The purpose of this experiment was to measure broadband low-frequency ocean basin backscattering from explosives and relate received pulses to individual bathymetric features. This report on the Levantine Sea basin is the second in a series of reports analyzing measured reverberation in various ocean basins.

Acoustic measurements were made with towed and vertical arrays to provide improved predictions of the true effects of underwater explosions on ASW sensors and missions, which is relevant to activated towed-array performance.

Results of the analysis showed backscattering in the Levantine Basin in the 100–715 Hz frequency region to be relatively well correlated with key bathymetric features in the basin even though the sources used were 0.818 kg SUS charges. Propagation conditions for the experiment were excellent, but both scattering strengths and reverberation-to-noise ratios were weaker than previous data for the Tyrrhenian Sea, which used depth charge sources. SACLANTCEN now has the capability to efficiently analyse basin reverberation, gather related reverberation statistics, and identify key scatterers within a basin. This analysis capability can be used to provide validation and tuning data for existing basin reverberation models. Such models could eventually be installed in NATO fleet tactical computers as decision aids.

Since the long-range objective of this effort is to achieve a thorough understanding of basin reverberation where heavy explosives can produce long-lasting reverberation in an ocean basin, there are several recommendations for future work. Data will be collected and/or analyzed in other areas so that similar analysis can be done on other ocean basins of interest. Work recommended includes bistatic measurements, which are needed for a full description of the scattering process. Propagation models that treat the two-way propagation loss problem should be developed to improve our understanding of the existing results. An experiment that carefully measures the forward and backscattered fields is needed to formulate inputs to scattering models.

intentionally blank page

Analysis of basin backscattering in the Levantine Sea

J. Preston, T. Akal and S. Fiori

Abstract: Research has been conducted in the Levantine Sea basin to measure low-frequency basin reverberation and relate the measurements to backscattering strength. The receivers were a towed horizontal array and a suspended vertical array. SUS (0.818 kg) charges were used as sources. In this broadband basin, reverberation data were collected simultaneously from the towed and vertical array. The towed-array data were taken on multiple headings; combining different headings permitted removal of the ambiguous directionality information from the towed array. Frequency domain beamformed data are presented for 100, 300, 450 and 715 Hz. Estimates of backscattering strengths of different features are provided and are in the range quoted in other publications. Statistics for the dominant backscatterers are given, relating scattering strength to incident angles on slopes.

Keywords: backscattering ○ explosives ○ Levantine basin ○ low-frequency reverberation ○ SUS charges

Contents

1 Introduction

The SACLANT Undersea Research Centre (SACLANTCEN) has been conducting research to improve the understanding of explosives-induced ocean basin reverberation. High acoustic source levels associated with heavy explosives can reverberate in a basin for extended periods. This report describes the data reduction and analysis associated with the first simultaneous measurements using towed- and vertical-array recordings of a series of SUS charges detonated in the Levantine Sea in June 1986. The experiment had two purposes. The primary purpose was to measure low-frequency basin reverberation and use the towed-array measurements to compute different basin features' backscattering strength and location. The other purpose was to compare explosives-induced backscatter measurements from a towed array with measurements from the vertical array. The experiment has had some results reported previously [1]. New data analysis tools are used in this report to present the experimental results in greater detail and to provide a somewhat different look at those results. The output of this work, which is a set of results that can be used for the validation and tuning of basin reverberation models, is relevant to anyone interested in lower frequency backscattering measurements.

2

Geometry and equipment description

Figure 1 shows the Levantine Sea basin bathymetry and the general site for the experiment, location R. The measurement site was located at 35°10′N, 30°10′E. Figure 2 shows a plan view of the experiment and the towed-array ship track. A towed horizontal array was deployed and positioned along one of a set of preselected headings at a depth of $\sim$ 100 m by the SACLANTCEN research vessel, the *Maria Paolina G.* (MPG). A vertical array was moored at the center of the experiment area. Data were collected simultaneously by the towed and vertical array, both of which had 32 hydrophones. The vertical-array midpoint was at a depth of 196 m. The hydrophones in both arrays were equally spaced and the total acoustic aperture for the two arrays was about 61 m in the low-frequency configuration (below 375 Hz) and half that for frequencies between 375 and 750 Hz. Data were processed at 100 and 300 Hz using the large aperture configuration. Data were also processed at 450 and 715 Hz using the higher frequency array with half the aperture. SUS charges were deployed from the MPG while on each of the straight legs of the track shown in Fig. 2.

The hardware used for data collection and processing is shown in Fig. 3. The major elements were the signal conditioning units (SCUs), the A/D converters, the high-density digital recorders (HDDRs), and the interpolator beamformer that filtered the data.

The acoustic conditions during the experiment are given in detail in Appendix A. They revealed a summertime propagation condition that coupled energy into the sound channel and resulted in fairly low propagation loss for this experiment.

Data processing for both the towed- and vertical-array data is described in Appendix B.

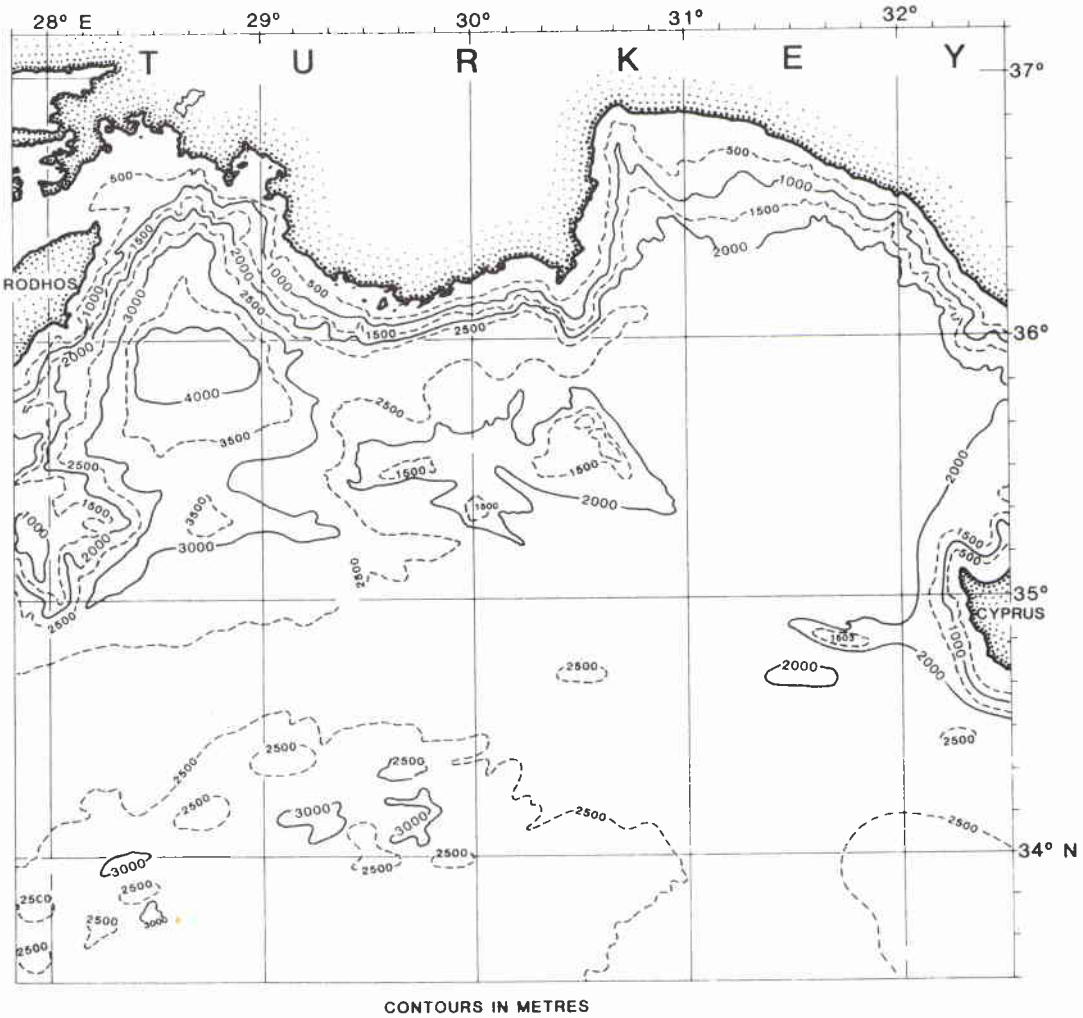

Figure 1 *Levantine basin backscattering experiment area bathymetry. The arrays are located near point R.*

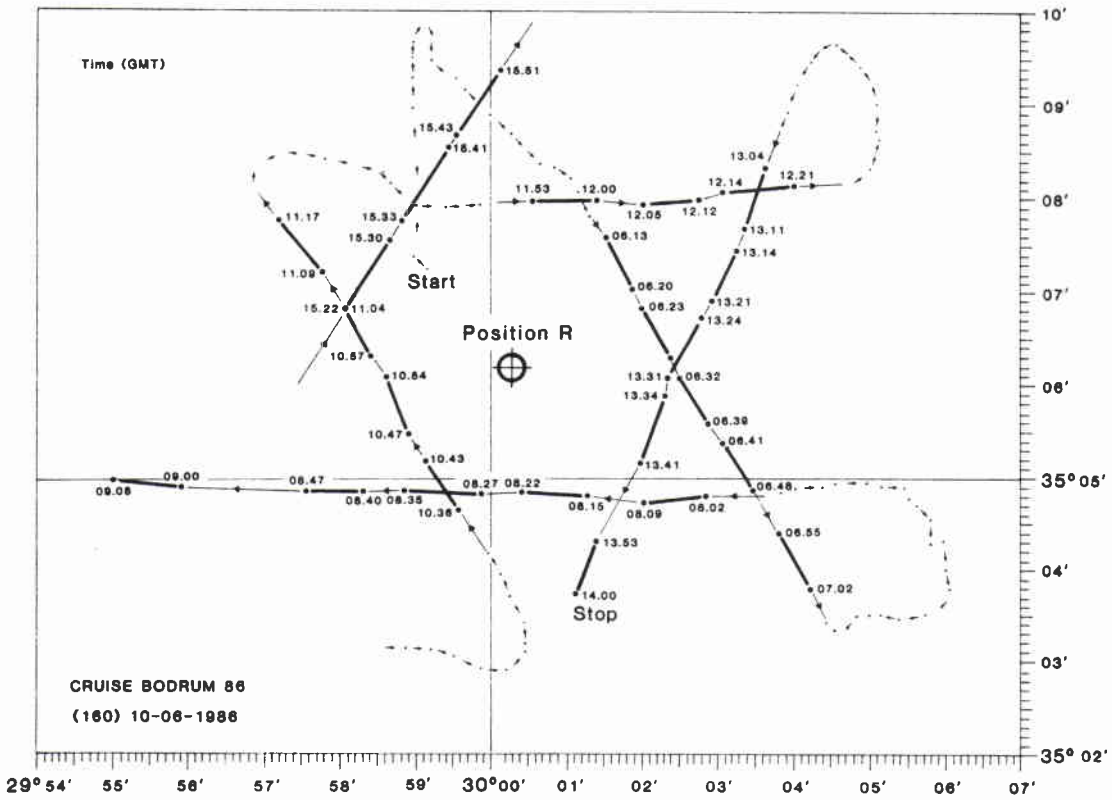

Figure 2 *Plan view of the basin backscattering experiment: showing the source receiving geometry with one shot on each leg of the ship track; vertical array at point R.*

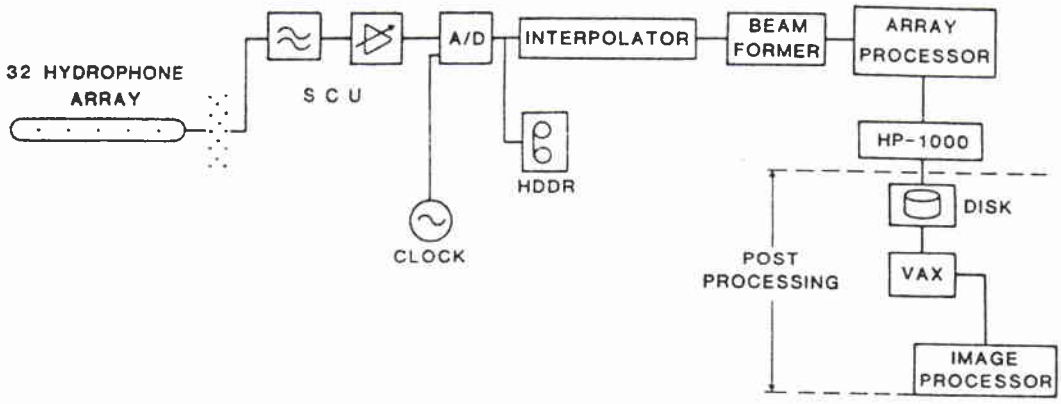

Figure 3 *Block diagram of SACLANTCEN's data acquisition and processing system for reverberation measurements.*

3
Results

Twenty-three SUS charge events were conducted but many were along nearly redundant headings and some others had recording problems. Five SUS charge events were selected for analysis and are referenced by numbers 1,2,3,4 and 5 in the subsequent discussion.

3.1. VERTICAL-ARRAY BACKSCATTER DATA

Vertical-array recordings of the reverberation have been analysed for event 2. Some two-dimensional fast fourier transform (FFT) beamforming results are presented in Figs. 4a–d for event 2 at frequencies of 100, 300, 450 and 715 Hz, respectively. For the vertical array, $+90°$ is upward endfire. Figure 4a also includes an overlay plot of level *vs* time to indicate some of the major reflectors in the basin and their relative levels. (This information was obtained with the help of towed-array results, which will be discussed in Sect. 4.)

The 300 and 715 Hz data shown in Figs. 4b and d are the most suitable data for estimating the arrival angle of energy incident on the vertical array. For an array of length L, L/λ (proportional to inverse beamwidth) of the array is ~ 4 at 100 Hz. So, the arrival angle resolution is much less than it is at 300 Hz. Nevertheless, a few distinct reverberation events can be seen over the 410 s of recorded 100 Hz data that are displayed in Fig. 4a. Reverberation arrivals in the Levantine basin tended to manifest themselves as the higher level energy bursts having durations typically from 10 to 30 s.

The 300 Hz plot (Fig. 4b) shows that for the two reverberation events that came in ~ 175 and 280 s after the direct arrival, the received angular spread in energy is $\sim \pm 10°$ for the reverberation. The received noise spread was $\sim \pm 14°$. In Fig. 4d (715 Hz) the observed angular spread of energy after 40 s appears to be due entirely to received noise and is therefore not useful in the present context.

Ray theory can be used, together with the above noted angular spread at 300 Hz, to postulate a bound on mean grazing angles of backscattered energy at long ranges. (Refer to the sound-speed profile, Table A1, in Appendix A.) The sound speed at a mean receiver depth of 196 m was 1513.8 m/s. A $\pm 10°$ ray at 196 m will be refracted to $0°$ when the sound speed becomes 1537 m/s; this corresponds to a water depth

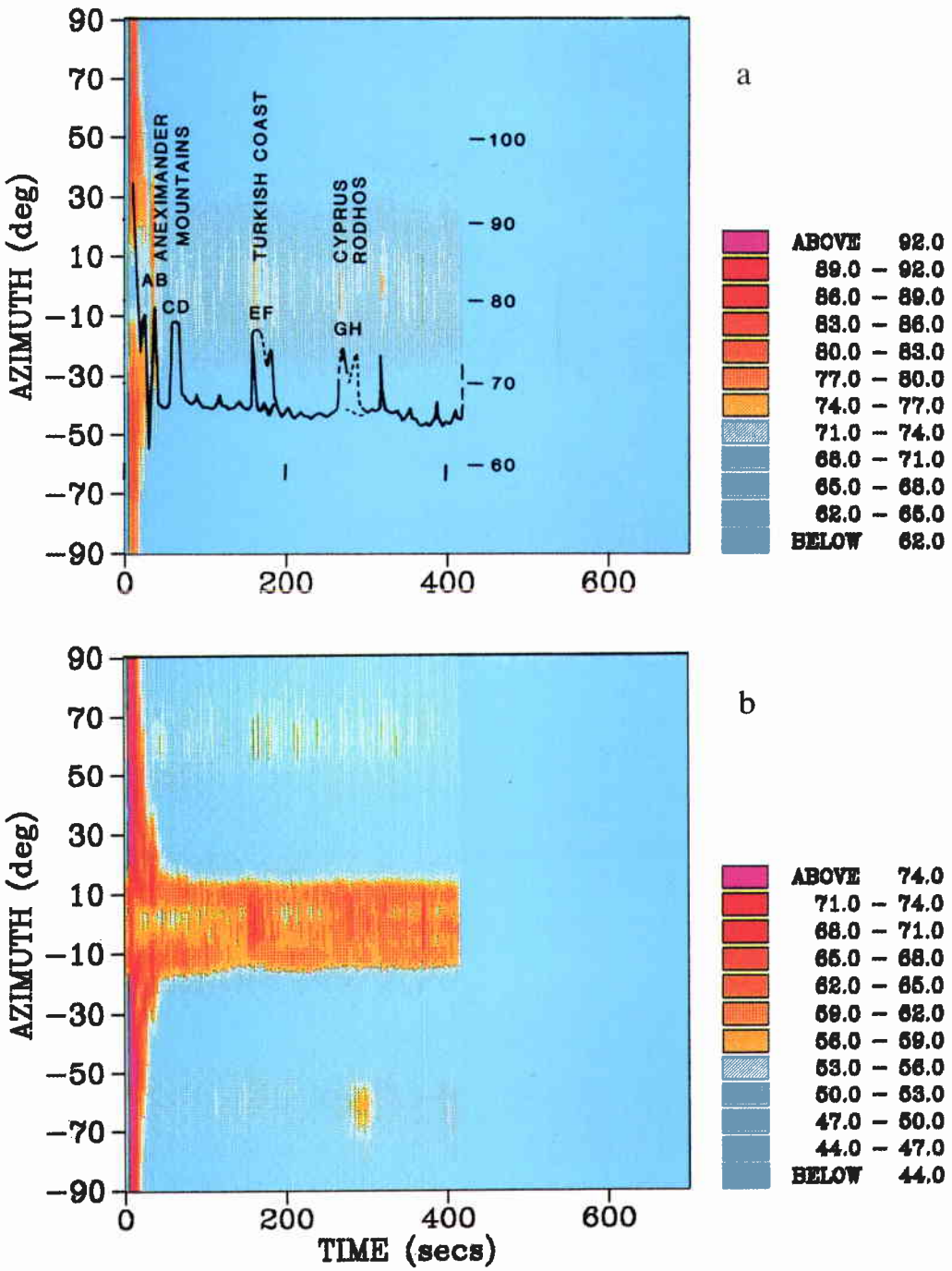

Figure 4 *Beam power vs angle and time for the vertical array: event 2 at (a) 100 Hz and (b) 300 Hz.*

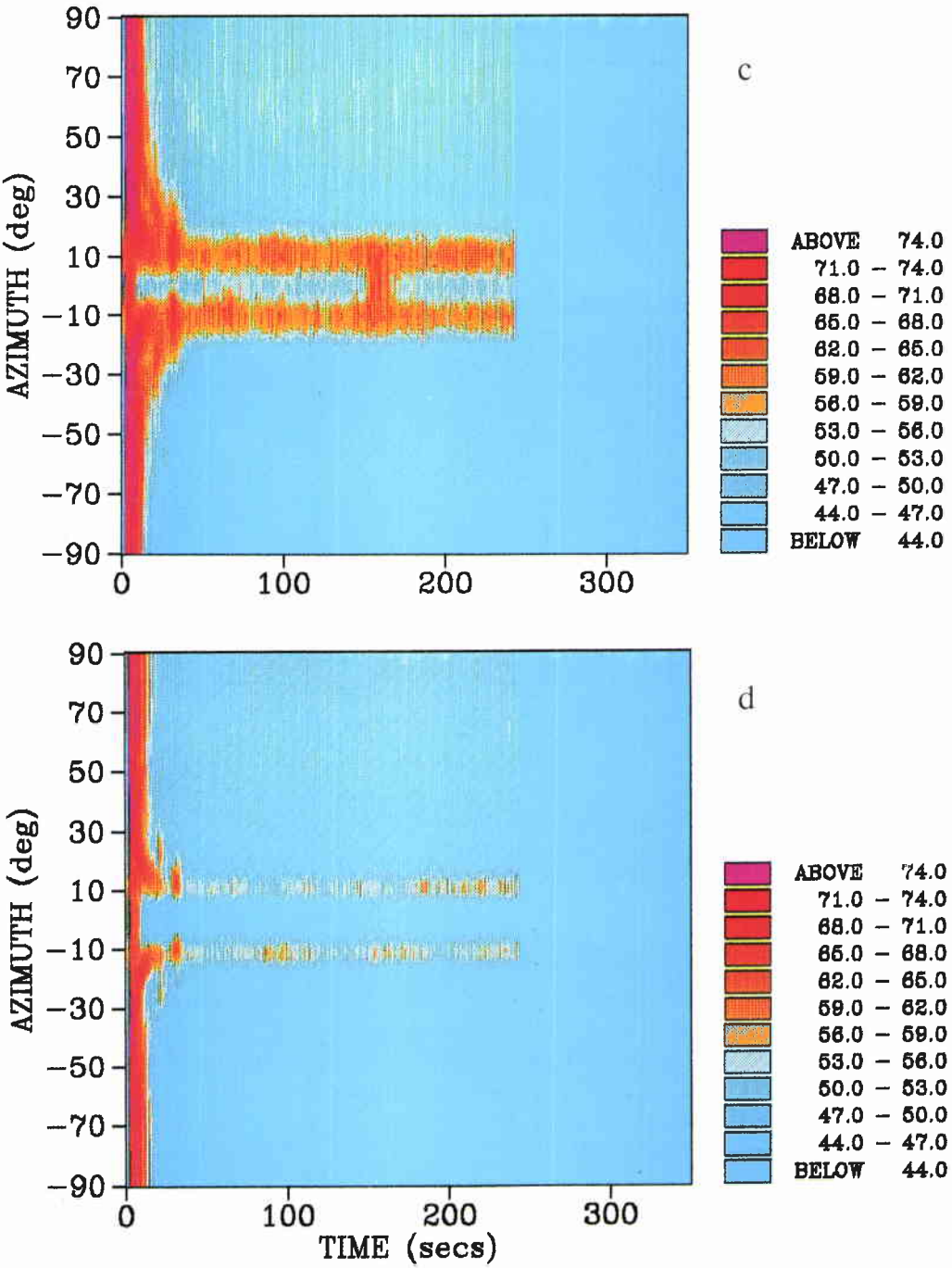

Figure 4 *Beam power vs angle and time for the vertical array: event 2 at (c) 450 Hz and (d) 715 Hz.*

of 1935 m. It is somewhat above the the sea-floor depth at the measuring site of $\sim$ 2300 m. Figure 5 shows this pictorially together with a graph of the sound-speed profile.

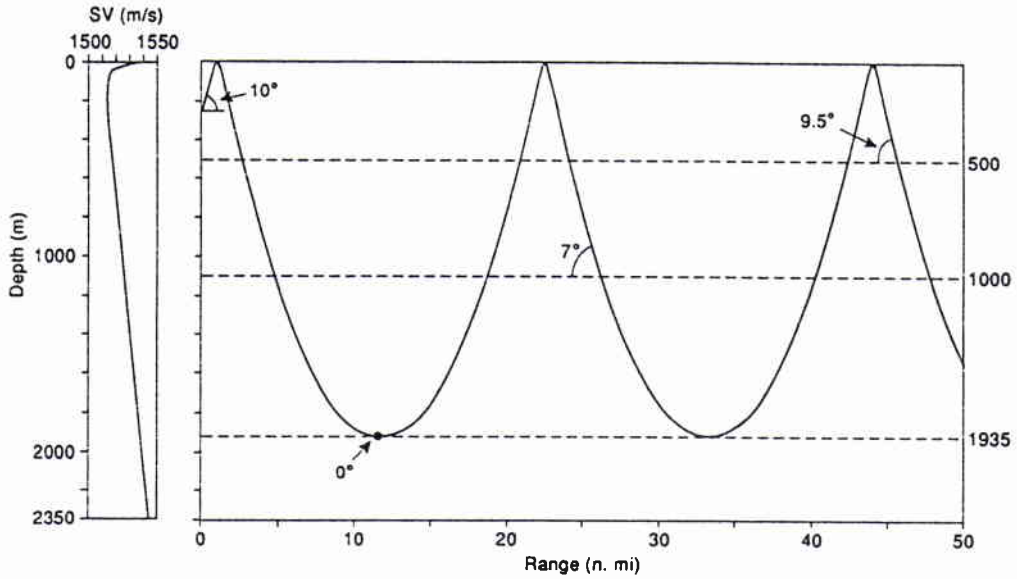

Figure 5 *Sound-speed profile and $-10°$ ray diagram showing intersection angles over likely bathymetric feature depths from 500 to 1900 m.*

Snell's law also implies that a $\pm 10°$ ray at 196 m would be refracted to a 7° incident angle on a continental margin at 1100 m depth (also shown in Fig. 5). The range of incident angles on the continental margins and seamounts over a 500–1900 m depth would be approximately between 9.5° and 0° relative to a horizontal line. For continental margins, average slopes in the 2–6° range are probable reverberation contributors [3]. This gives an estimated spread of relative incident angles on these slopes of $\sim$ 2–16° (relative to the slope itself). In [2], it is shown that some slopes can reach 15° or more over short distances.

Appendix A shows results from raytrace and the SACLANTCEN parabolic equation model (PAREQ) [4] runs for this environment (Figs. A3–A5). Based on these model runs, much of the vertical distribution of waterborne energy is in the upper 1200 m of the water column. (However, this does not hold for ranges less than $\sim$ 20 km.)

3.2. TOWED-ARRAY BACKSCATTER DATA

This section describes results for the towed array for the five selected SUS events and how these results are used to determine scatterer position.

Processing similar to that done for the vertical array was also done for the towed array as a first step to extracting even more information from the towed-array data. Unlike the vertical-array data, individual reverberation arrivals can be directly associated with a particular relative bearing at specific times. Rectangular-azimuth *vs* time plots for the towed array were converted to latitude and longitude so that the received reverberation would overlay a chart like Fig. 1. This conversion involved a conformal transformation using known mapping transformations [5] to the mercator chart of Fig. 1. The approximation of a collocated source and receiver has been made for this algorithm and so the source-receiver baseline of slightly less than 1 km has been neglected.

Using a technique similar to those outlined in [6–8], the beam power, in dB, from several different array orientations can be averaged to effectively remove the ambiguity and improve angular resolution of a backscatter. Figures 6a–d show the result of this averaging for the 100, 300, 450 and 715 Hz cases, respectively, over five selected array headings. The orientation and array positions are also indicated on the figure. (Each line length represents the travel distance for two-way travel of a sound pulse after 50 s.) A midpoint source-receiver location was assumed as the single reference point; therefore the results have been averaged over about a 2.5 km area. A transparent overlay of Fig. 1 is superimposed on the backscattering plots.

The backscatter energy is seen to correlate well with the location of rising slopes from coastal margins and seamounts. Relatively strong scattering is evident primarily at the three lowest frequencies analysed (100, 300 and 450 Hz). Higher level energy can be seen on these plots, which remain constant along a given bearing; it is usually towship noise that was not completely cancelled out by this technique.

3.3. MONOSTATIC BACKSCATTERING ESTIMATES

This section expands the processing described in Subsects. 3.1 and 3.2, to include scattering-strength determination as a function of position and frequency. Figure 7 is the methodology flowchart. (Single frequency data processing was described in Appendix B and the scatter position algorithm was described in Subsect. 3.2.)

For the towed array, a simple model of the basin backscattering process was constructed [2] using the active sonar equation for reverberation from an elemental area patch [9]. Then one can transform the plots in Subsect. 3.2 into estimates of backscattering strength as a function of range and azimuth. The transmission loss was assumed to be $20 \log R + \alpha R$ out to 6500 m and $10 \log R + \alpha R$ thereafter. (See [2] for a comparison of this with PAREQ and measured data and also for a more detailed

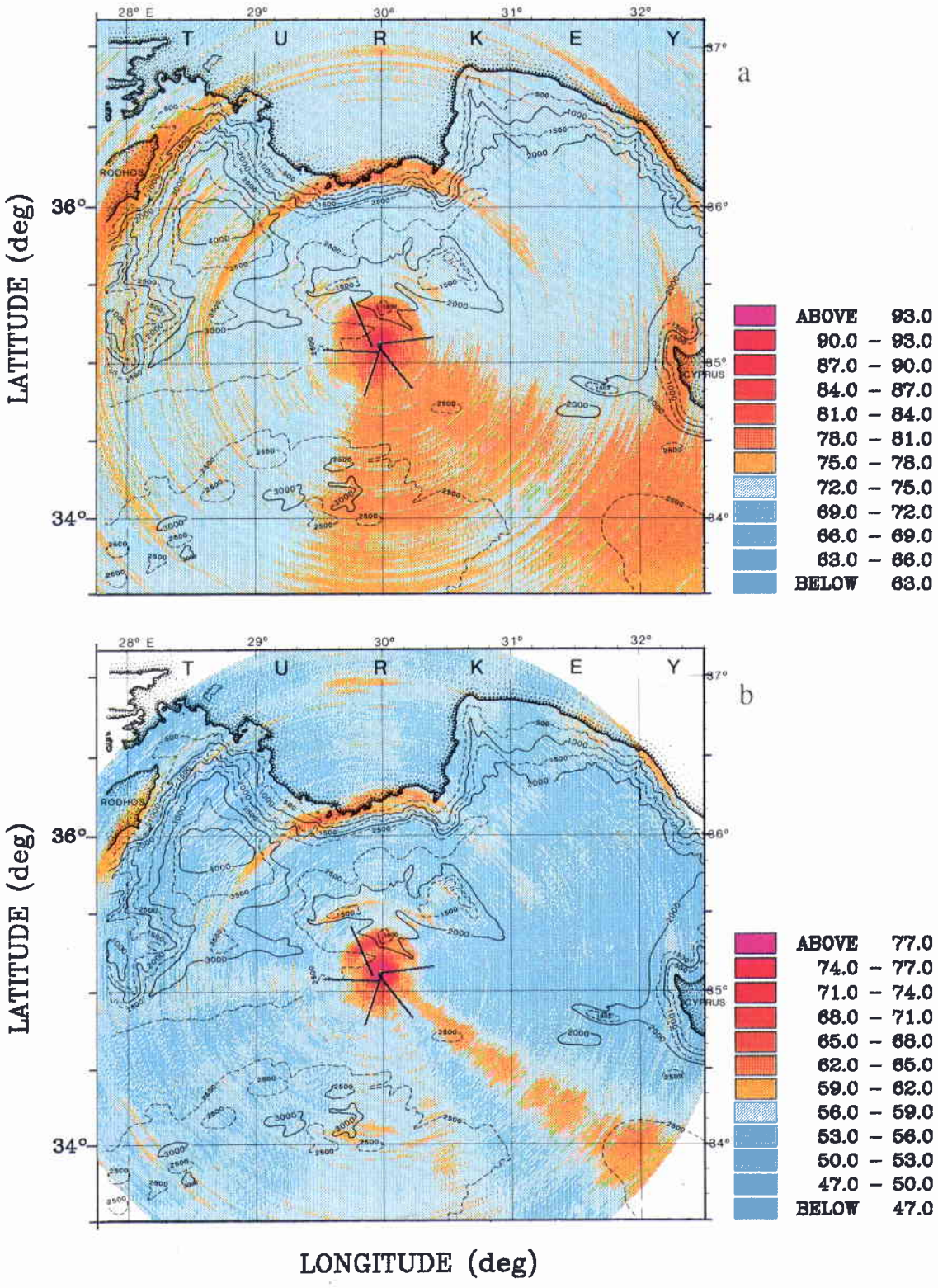

Figure 6 *Received beam power vs location for the towed array: sum over 5 events at (a) 100 Hz and (b) 300 Hz.*

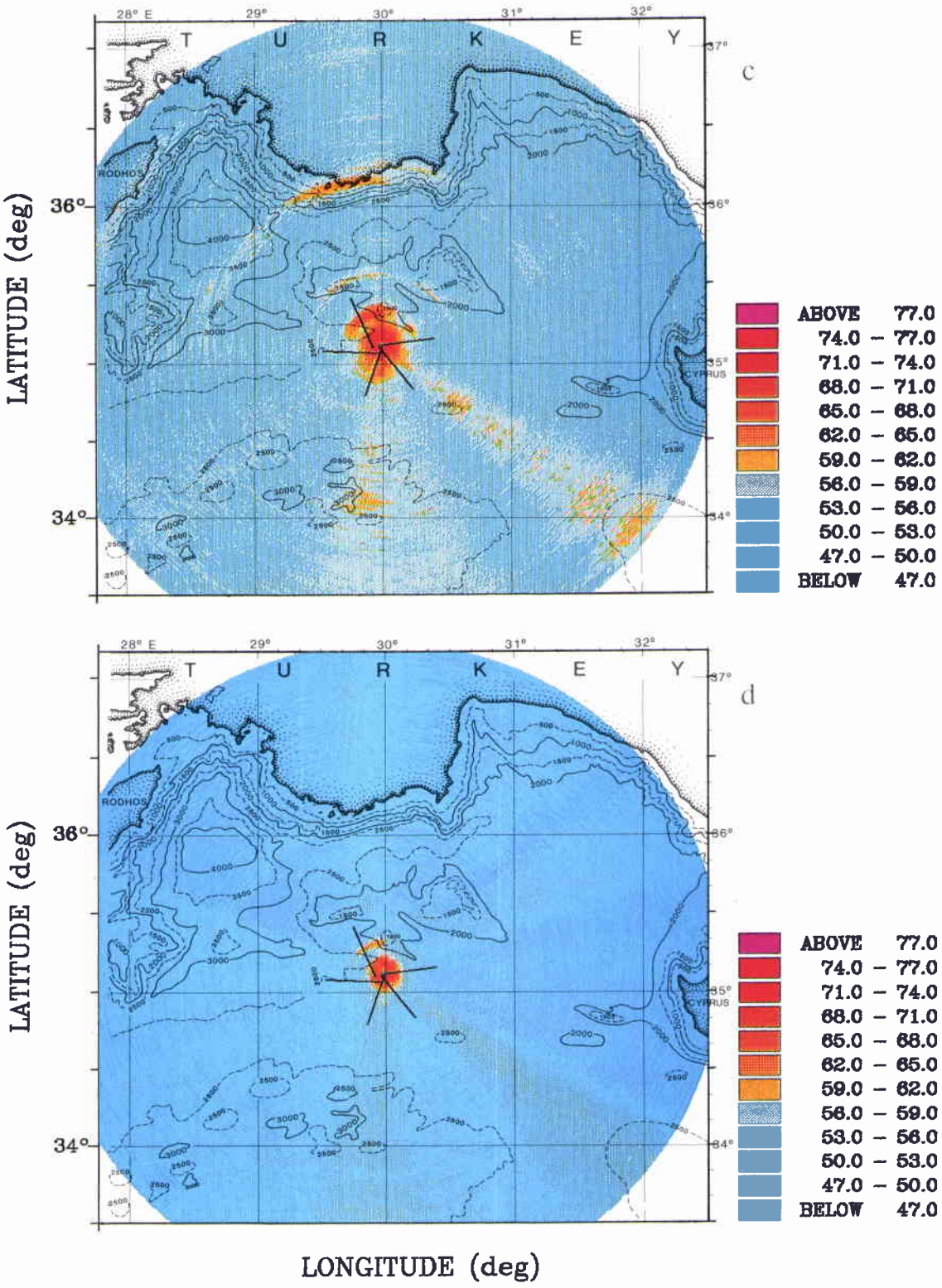

Figure 6 *Received beam power vs location for the towed array: sum over 5 events at (c) 450 Hz and (d) 715 Hz.*

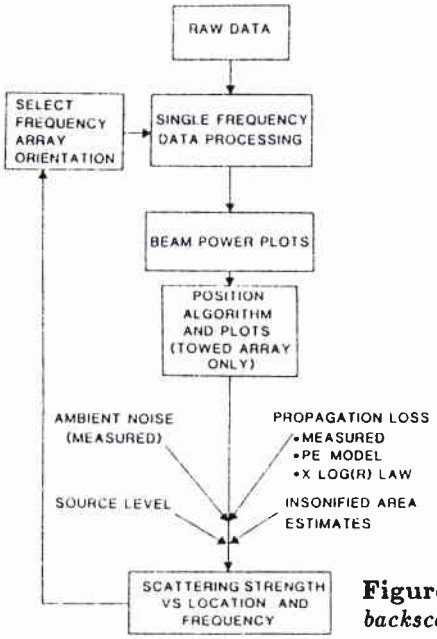

Figure 7 *Methodology flowchart for basin backscattering.*

explanation of the assumptions and limitations of this method.) The analysis time window T was 512/750 Hz sample rate = 0.6827 s for the 100 and 300 Hz analysis and 0.3415 for the 450 and 715 Hz analysis. The beamwidth was taken from Urick [9] for an equally spaced array and multiplied by 1.5 for a Hann window correction.

Figures 8a–d show the result of combining the four events with different headings to obtain an estimate of backscattering strength at 100, 300, 450, and 715 Hz, respectively, that has removed the array ambiguity and most of the towship noise. Unlike Fig. 6, the estimated noise has been subtracted before backscatter strengths were computed. The backscattering strengths for the stronger scatterers shown in Fig. 8 range from -25 to -35 dB and are consistent with the results quoted for these frequencies in other papers [1–3,6,8,10]. Figures 8a–d also show good correlation between high values of scattering strength and the major bathymetric features of the basin.

Using a methodology previously described [1,2], it is possible to construct a comparison of towed- and vertical-array scattering strength estimates. In fact, this was already done [1] for selected scattering features using this data set. In addition, a similar comparison was made for a set of data taken in the Tyrrhenian Sea [2]. Figure 9 shows results of these comparisons from the two Mediterranean basins on one graph. One can see that the greatest variability with frequency comes from the Turkish coast segment.

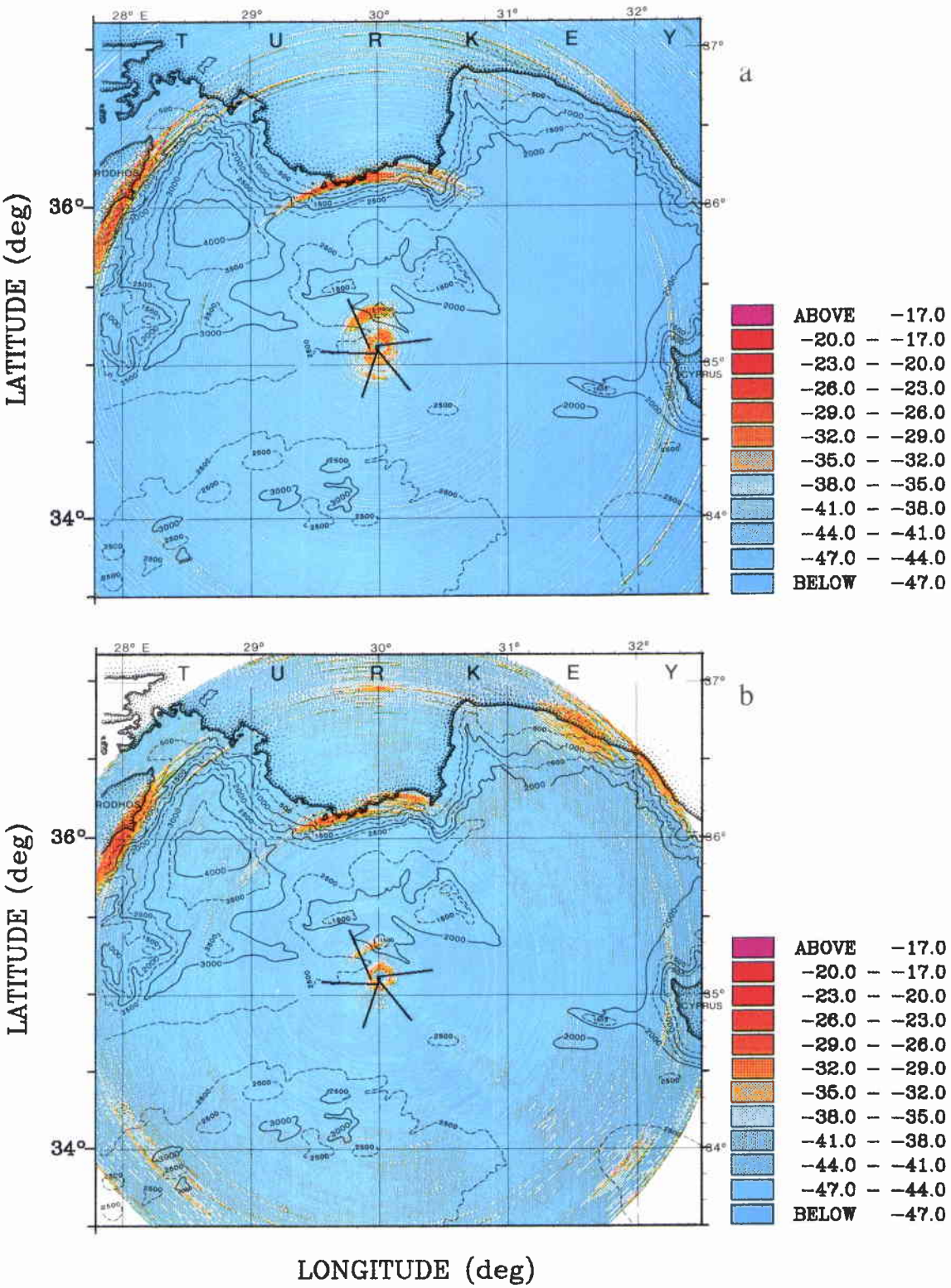

Figure 8 *Estimated backscattering strength vs location, from average over 4 events at (a) 100 Hz and (b) 300 Hz.*

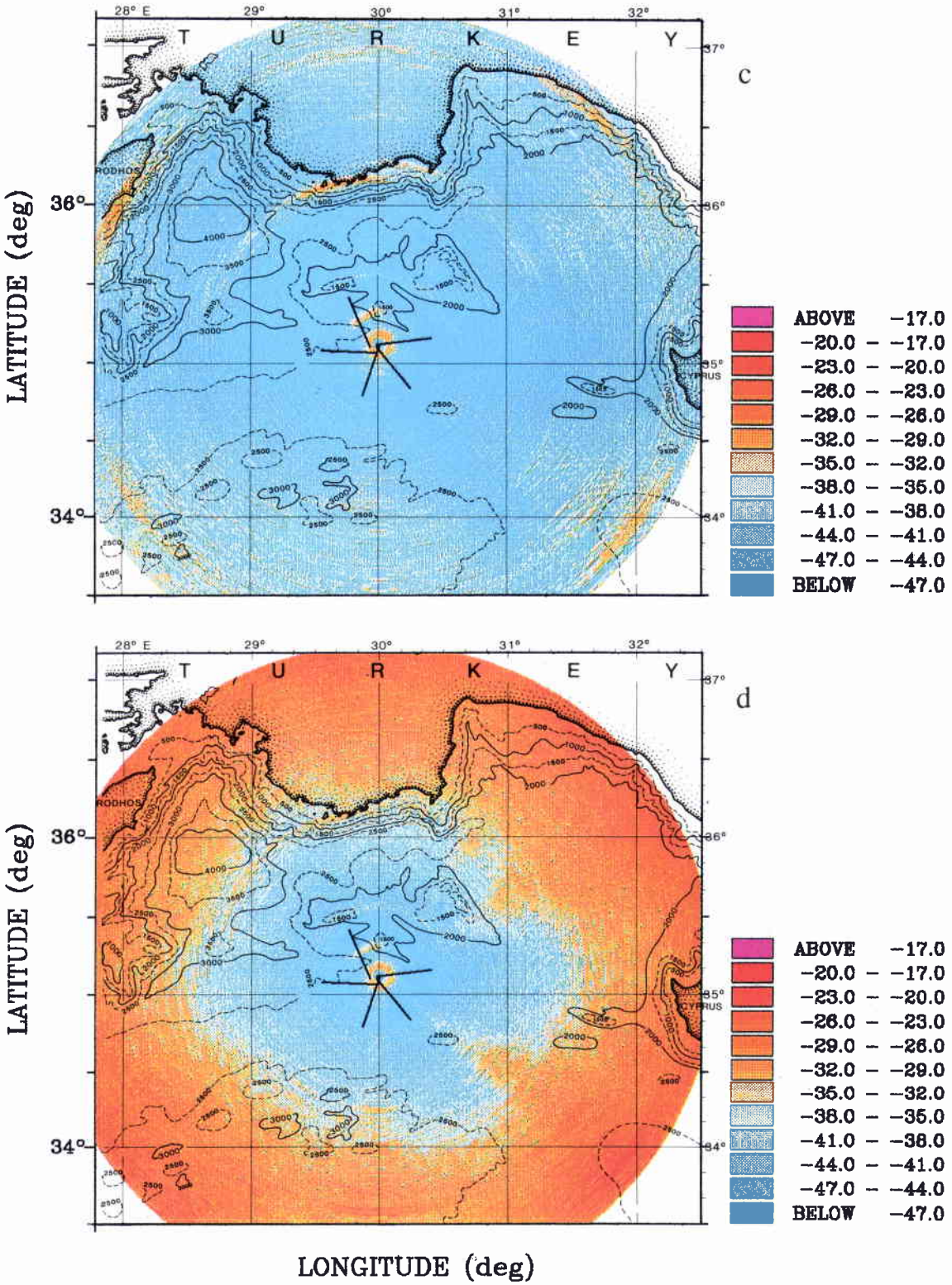

Figure 8 *Estimated backscattering strength vs location, from average over 4 events at (c) 450 Hz and (d) 730 Hz.*

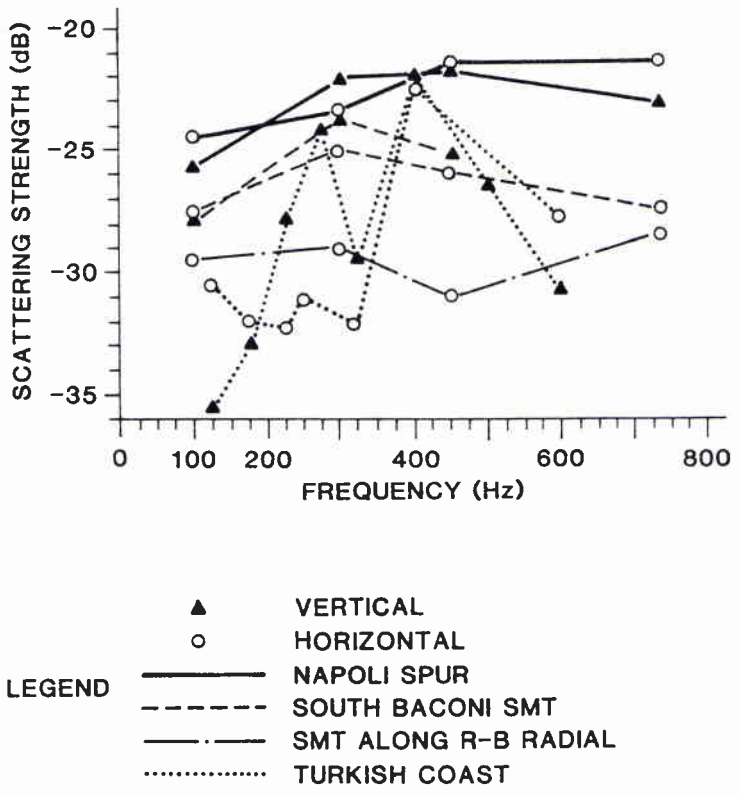

Figure 9 *Comparison of estimated backscattering strength vs frequency for the SACLANTCEN towed and vertical arrays. Taken from data in the Tyrrhenian and Levantine basins.*

3.4. STATISTICS ON THE BACKSCATTER DATA

The final step in this data analysis was to use an image segmentation algorithm developed previously [2], to separate automatically, individual scatterers appearing on the polar displays and compute statistics on those masses which satisfied certain threshold requirements. Thresholds were selected for the number of contiguous pixels in a display that were above a certain scattering strength; −35 dB was selected as the scattering strength threshold for this data set. A contiguous mass threshold of 20 pixels was the other threshold selected. The mean and standard deviation of levels in dB were computed for the pixels in each mass. The peak scattering strength in the mass, the area of the observed mass size of the scatterer in km^2 and the range and bearing to the centroid of the mass were also computed. Arrivals from less than 10 km were removed from the statistical computations, as were arrivals over land masses. The results of these computations are shown in Table 1 for the 22 masses identified in the 300 Hz display of Fig. 8. These statistics for the scattering strengths are averaged over the five events selected previously.

Histograms were plotted of the peak averaged scattering strengths (from Table 1)

Table 1 *Scattering strength statistics*

Mass no.	No. pts.	Average (dB)	Std. dev. (dB)	Max. SS (dB)	Area (km^2)	Range (km)	Bearing (°)	Change in depth (m)	Slope (°)	Relative azim. angle (°)
1	36	−34.1	0.7	−32.6	39.06	120.6	9.4	1090.8	9.51	0.0
2	22	−34.3	0.5	−32.8	24.29	122.7	6.1	980.0	9.51	0.0
3	45	−33.5	1.0	−31.5	50.50	124.8	8.0	896.9	9.51	0.0
4	92	−32.9	1.4	−29.9	105.72	127.7	8.1	532.7	8.36	0.0
5	38	−34.1	0.7	−31.9	69.41	203.1	8.8	75.5	1.03	0.0
6	266	−32.4	2.1	−26.2	557.70	233.1	47.9	1071.0	8.11	0.0
7	194	−33.1	1.3	−30.1	382.83	219.4	37.5	1142.1	7.77	0.0
8	37	−33.9	0.6	−32.9	70.96	213.2	37.5	1185.8	7.19	1.0
9	95	−33.0	1.1	−30.8	193.10	226.0	38.5	624.4	7.96	0.0
10	32	−33.6	0.8	−32.1	66.18	229.9	38.7	164.2	2.91	0.0
11	50	−33.1	1.1	−31.2	105.63	234.9	121.7	540.5	5.20	0.5
12	30	−32.6	0.9	−31.6	58.04	215.1	128.5	220.0	0.83	85.3
13	52	−32.6	1.2	−30.1	109.61	234.3	216.4	399.3	1.79	0.0
14	24	−33.0	1.0	−31.1	42.36	196.2	218.3	184.1	0.93	49.9
15	25	−34.2	0.7	−32.8	42.78	190.2	230.0	465.9	2.27	71.1
16	48	−33.8	1.0	−31.2	89.28	206.8	234.5	508.8	2.25	0.0
17	645	−31.8	2.2	−26.0	1169.34	201.5	300.1	2160.1	12.65	0.0
18	29	−33.9	1.2	−31.5	55.04	211.0	288.7	627.2	4.76	5.6
19	266	−33.5	1.0	−31.4	51.39	21.5	334.8	804.6	3.68	3.9
20	23	−33.5	0.8	−32.2	39.66	191.7	322.3	2529.5	7.50	1.8
21	331	−31.8	1.9	−25.4	342.66	115.1	344.9	1652.1	9.50	4.8
22	24	−34.6	0.2	−34.1	5.31	24.6	344.6	238.9	3.28	60.4

Overall average: −33.3; Range of maximum scattering strength: −34.1 −25.4.

and the backscatter area, as measured by the area of the identified mass in km^2, which exceeds −35 dB. These results are shown in Fig. 10. Area intervals were selected to be multiples of 2 and would correspond to 3-dB steps if used in the sonar equation (assuming a pulse length > the feature extent in range). Because statistics are in dB the peak averaged level over 5 events +10 log of the area is probably closer to estimating the total backscatter from a feature than using the mean level +10 log of the area. The first method is an upper bound and the second a lower bound of the total backscatter from a feature that is more correctly estimated as an integral or sum over the feature.

Table 1 also reflects the fact that a link has been established with bathymetric data bases. For a given mass, local slopes Θ_c and reflection angles relative to the receiver look direction Φ_r are computed using that link. The last two columns on the right of Table 1 display these angles. The third to the last column computes the change in depth over a selected feature (or mass) ΔD. After some trial and error it has been found that the product $\Delta D \sin\Theta_c \cos\Phi_r$ is reasonably correlated with the peak scattering strength over a feature. This quantity is linearly related to a crude estimate of the area of the feature facing the source/receiver. Figure 11 shows the result of a linear regression computation for the conditions stated above.

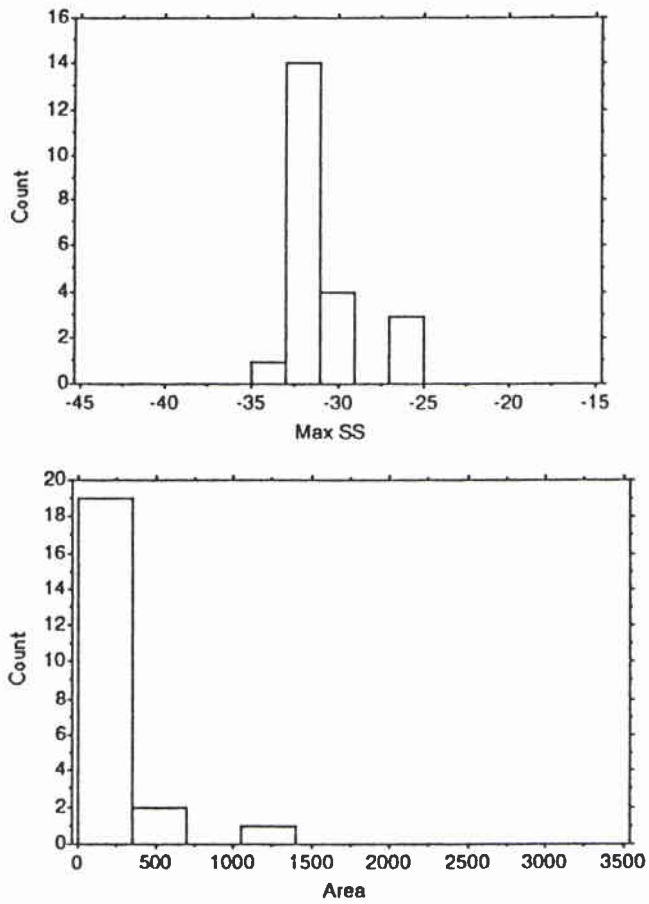

Figure 10 *Histograms of peak scattering strength (top) and backscatter area (bottom) at 300 Hz for all features above threshold of −35 dB (towed array only).*

In [10] very strong correlation between scattering strength and seamount heights were found in the Canary basin of the Atlantic. This Levantine basin data showed a weaker dependence on ΔD; however, both seamounts and basin segments are mixed into the correlations shown here.

The data presented apply to backscattering for point R in Fig. 1. Many features will probably backscatter somewhat differently with different azimuthal incidence angles. The measured scattering strength of a feature will depend to a certain extent on relative source and receiver measurement geometry. Nevertheless, the low-frequency backscattering estimates and statistics presented here are useful in estimating relative backscattering strengths of basin features and comparing results with other work. Therefore, they are of interest even in this simplified form.

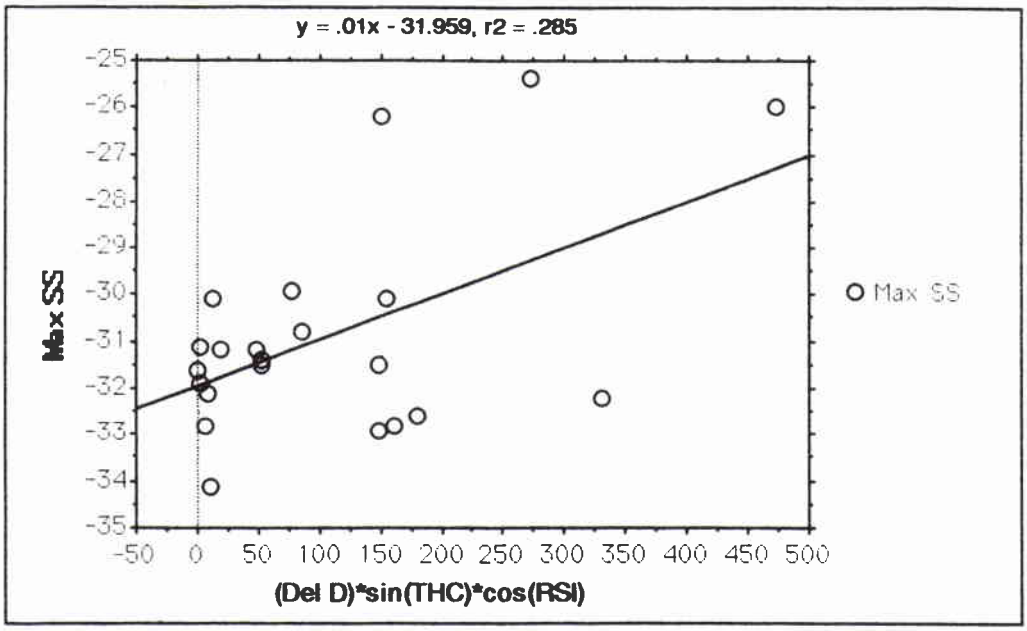

Figure 11 *Linear Regression of Maximum Scattering Strength vs* $\Delta D \sin \Theta_c \cos \Phi_r$ *(for features above threshold).*

4

Summary and conclusions

Levantine Sea backscattering data have been presented for both a towed array and a vertical array. As others have noted, backscattering is dominated by basin features where there is a substantial decrease in depth over a relatively short distance. An important result of this experiment is that useful backscattering results can be obtained with SUS charges with proper environmental conditions. Because propagation was primarily confined to the sound channel, the sea floor did not appear to backscatter much energy in the form of classic boundary reverberation when compared to the basin margins and seamounts. Nor was any obvious evidence of surface boundary reverberation observed (except in the first 20–40 s after the explosion), when the fathometer effect was probably dominant [2]. Basin backscattering statistics were presented and selected features isolated for further statistical analysis. Correlation of backscattering features with inherent and relative slope angles was presented and a promising independent regression variable was introduced which is a function of these angles. These results should also be useful for sonar performance computations involving reverberation between 100 and 800 Hz.

References

[1] Berkson, J.M. and Akal, T. Simultaneous reception of long range low frequency backscattered sound by a vertical and horizontal array. *IEEE Journal of Oceanic Engineering*, **12**, 1987: 362–367.

[2] Preston, J.R., Akal, T. and Fiori, S. Analysis of backscattering data in the Tyrrhenian Sea, SACLANTCEN SM-221. La Spezia, Italy, SACLANT Undersea Research Centre, 1989.

[3] Baggeroer, A. and Dyer, I. Long range, low frequency acoustic backscattering: A Survey. *In*: Akal, T. and Berkson, J.M. *eds.* Ocean Seismo-Acoustics: Low-frequency Underwater Acoustics. New York, NY, Plenum Press, 1986: pp. 313–326.

[4] Jensen, F.B. and Martinelli, M.G. The SACLANTCEN parabolic equation model (PAREQ). La Spezia, Italy, SACLANT Undersea Research Centre, 1985.

[5] Pearson, F. Map Projection Methods. Blacksburg VA, Sigma Scientific, 1984.

[6] Erskine, F.T., Bernstein, G. and Franchi, E.R. Imaging Techniques for analysis of long range acoustic backscatter data from ocean basin regions. *In*: Tollios, C.D., McElroy, M.K. and Syck, J., eds. Proceedings, 3rd Working Symposium on Oceanographic Data Systems. Piscataway, NJ, IEEE, 1983: pp. 160–164.

[7] Wagstaff, R.A. Iterative technique for ambient-noise horizontal-directionality estimation from towed line-array data. *Journal of the Acoustical Society of America*, **63**, 1978: 863–869.

[8] Dyer, I., Baggeroer, A.B., Zittel, J.D. and Williams, R.W. Acoustic backscattering from the basin and margins of the Arctic Ocean. *Journal of Geophysical Research*, **87**, 1982: 9477–9478.

[9] Urick, R. Principles of Underwater Sound. New York, NY, McGraw-Hill, 1983.

[10] Erskine, F.T., Franchi, E.R. and Adams, B.B. Seamount height estimation from long-range, low-frequency acoustic backscatter. *In*: Akal, T. and Berkson, J.M. *eds.* Ocean Seismo-Acoustics: Low-frequency Underwater Acoustics. New York, NY, Plenum, 1986: pp. 335–344.

[11] Nairn, A., Kanes, W. and Stehli, F. The Ocean basins and margins: vol. 4a: the Eastern Mediterranean. New York, NY, Plenum Press, 1977.

[12] Watkins, J.S., Montadert, L. and Dickerson, P.W. Geological and Geophysical Investigations of Continental Margins. Tulsa, American Association of Petroleum Geologists, Oklahoma, 1979.

Appendix A

Acoustic environmental conditions

This appendix summarizes the acoustic parameters measured and/or modeled for the June '86 experiment in the Levantine Sea to obtain backscatter levels and scattering strengths. This section is intended as general background information pertaining to the results in the main text.

Bathymetry and geology Figure 1 of the main text, shows the bathymetry for the experiment area. The basin features include a relatively thick sediment layer but with complex plate tectonics, creating topographic features with high impedance that can backscatter acoustic energy [11,12].

Acoustic propagation and the sound-speed profile Acoustic ray-tracing models were run for given source depths and sound speed *vs* depth profiles (SSPs). The water depth at the measurement site was ca. 2300 m. The sound-speed profile was calculated using a conductivity–temperature–depth sensor (CTD) and expendable bathythermographs (XBTs). Table A1 presents the sound-speed profile derived from the CTD data. Figure A1 shows the ray-path diagram for a source at 240 m (the explosion depth for this experiment). The predominant mechanism for long-range (> 60 km) propagation appears to be via refracted-surface-refracted (RSR) paths and refracted-surface-reflected-bottom-reflected (RSRBR) paths and so more bottom interaction should be present in these data compared with a previous data set from the Tyrrhenian Sea [2].

Table A1 *Measured sound-speed profile*

Depth (m)	Sound speed (m/s)	Depth (m)	Sound speed (m/s)
0	1534.2	100	1514.7
10	1534.3	200	1513.8
20	1528.0	300	1514.2
30	1522.0	400	1514.5
40	1519.5	500	1515.5
50	1517.5	700	1518.3
60	1516.5	1740	1534.6
70	1515.5	2300	1543.3
80	1515.0		

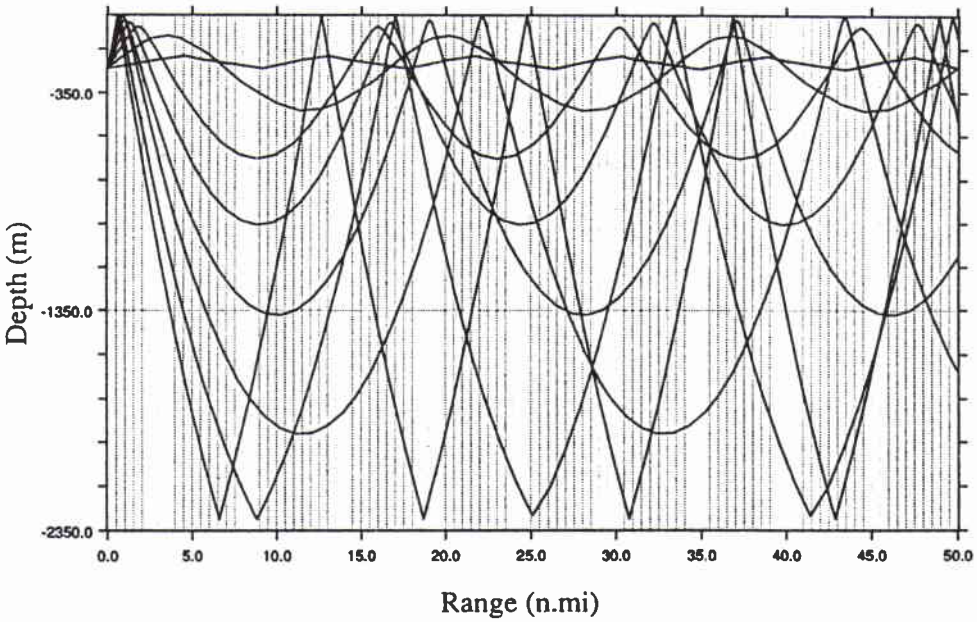

Figure A1 *Ray diagram for a source depth of 240 m (0–16° at increments of 2°).*

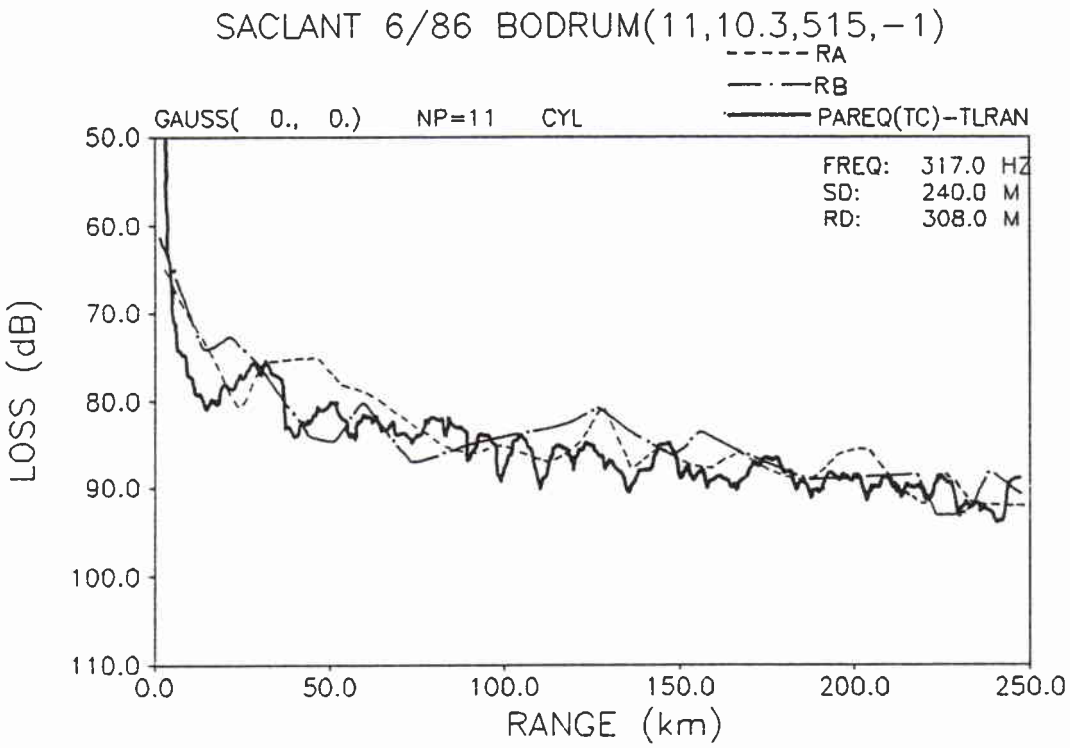

Figure A2 *Comparison of measured and modeled propagation loss at the receiver site R for 317 Hz; source at 240 m and receiver at 308 m.*

The SSP of Table A1 was used as an input to the SACLANTCEN PAREQ propagation loss model to compare transmission loss predictions with measured data. This model uses a parabolic approximation to the full-wave equation to compute the change in intensity as a function of depth and range. Figure A2 shows a comparison of measured and PAREQ estimated propagation loss for a source at 240 m and receiver at 308 m at 317 Hz. Runs RA and RB represent radials outward from point R of Fig. 1 along 255° and 140°, respectively. Considering the variation of data with azimuth, the agreement between model and data is good and is usually less than 5 dB. This model run was made assuming range independent bathymetry and sound speed.

Model runs of intensity *vs* depth indicated that much of the time energy is in the upper 2500 m of the water column. The rising continental margins often extend to depths < 500 m. Hence, for the purposes of estimating propagation loss *vs* range in both directions along a backscatter path, some PAREQ predictions were run for a receiver depth of 1150 m. This is very roughly a midpoint estimate of an interaction depth for RSR rays intersecting a rising continental margin or seamount base and being backscattered to the receiving arrays.

Figures A3 and A4 show the results of the PAREQ model computation for a source at 240 m and receiver at 1150 m and 300 m, respectively, at a frequency of 300 Hz. Loss *vs* range curves often show distinct convergence zones every 30–70 km in range. However, the loss *vs* range curves in Figs. A3 and A4 show a fairly smoothly decaying range dependence with convergence zones seeming to occur more or less at random. Also shown for comparison in Fig. A3 is the cylindrical spreading curve used to compute scattering strength (deep receiver assumed). A crossover range from spherical to cylindrical spreading for that curve was taken as 6500 m.

Figure A5 shows a 300 Hz contour plot of loss *vs* range for the constant bottom depth of 2300 m. Only very shallow receivers are predicted to show a low loss from a source at 240 m in this environment. Propagation to receivers below ~ 500 m shows much higher losses and weak local maxima and minima with range.

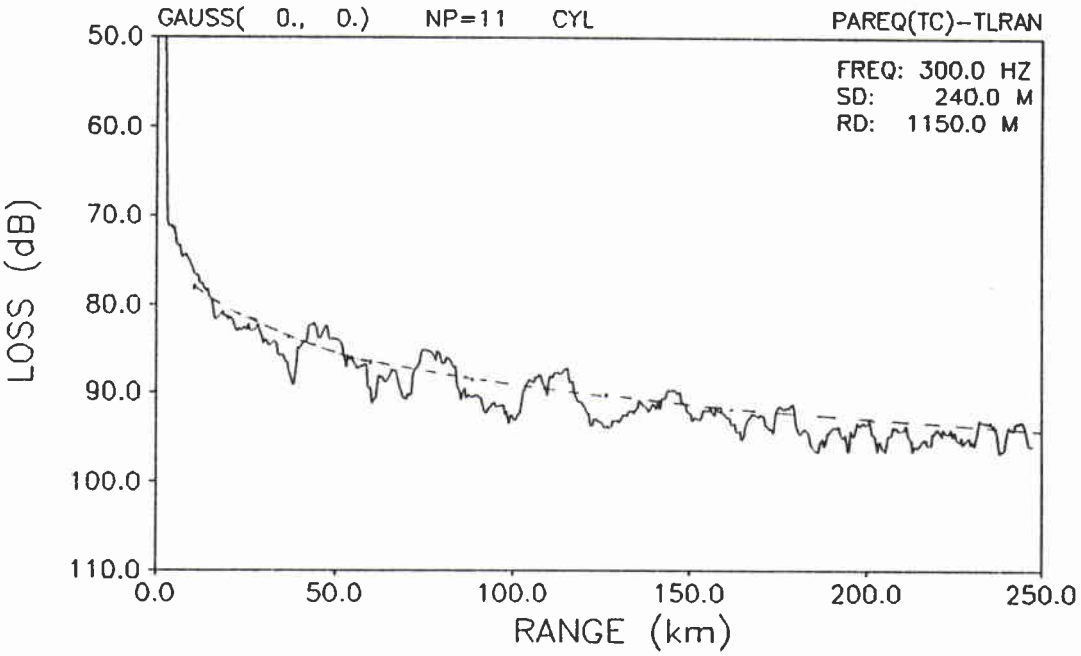

Figure A3 *Predicted propagation loss for source at 240 m and receiver at 1150 m, at 300 Hz. (The solid curve shows the* PAREQ *predictions, while the dashed line shows cylindrical spreading.)*

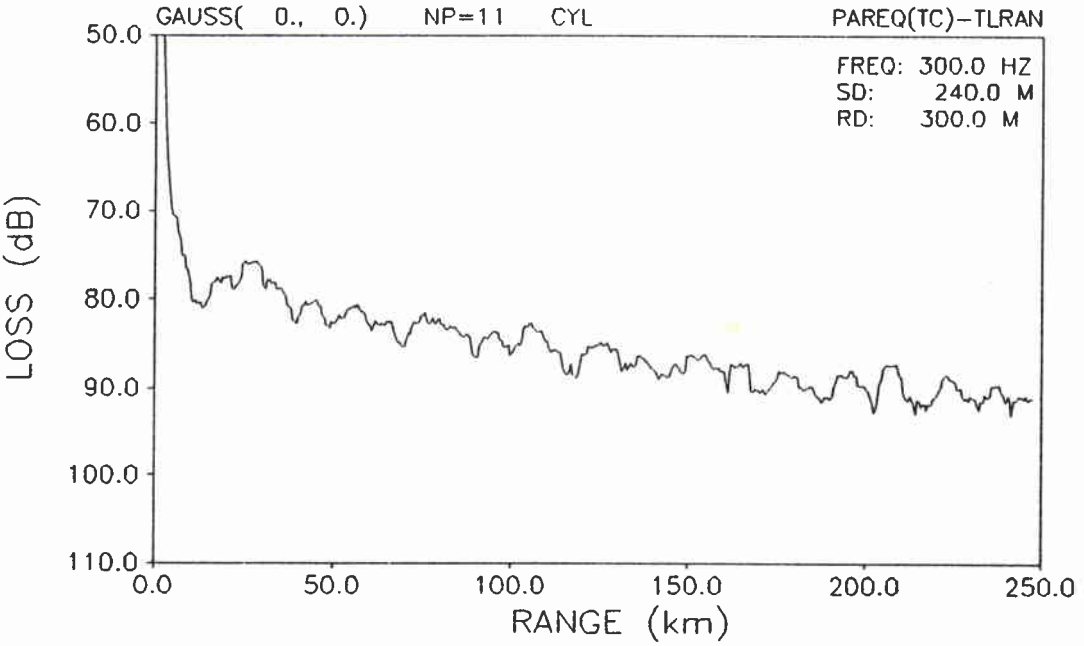

Figure A4 *Predicted propagation loss for source at 240 m and receiver at 300 m, at 300 Hz.*

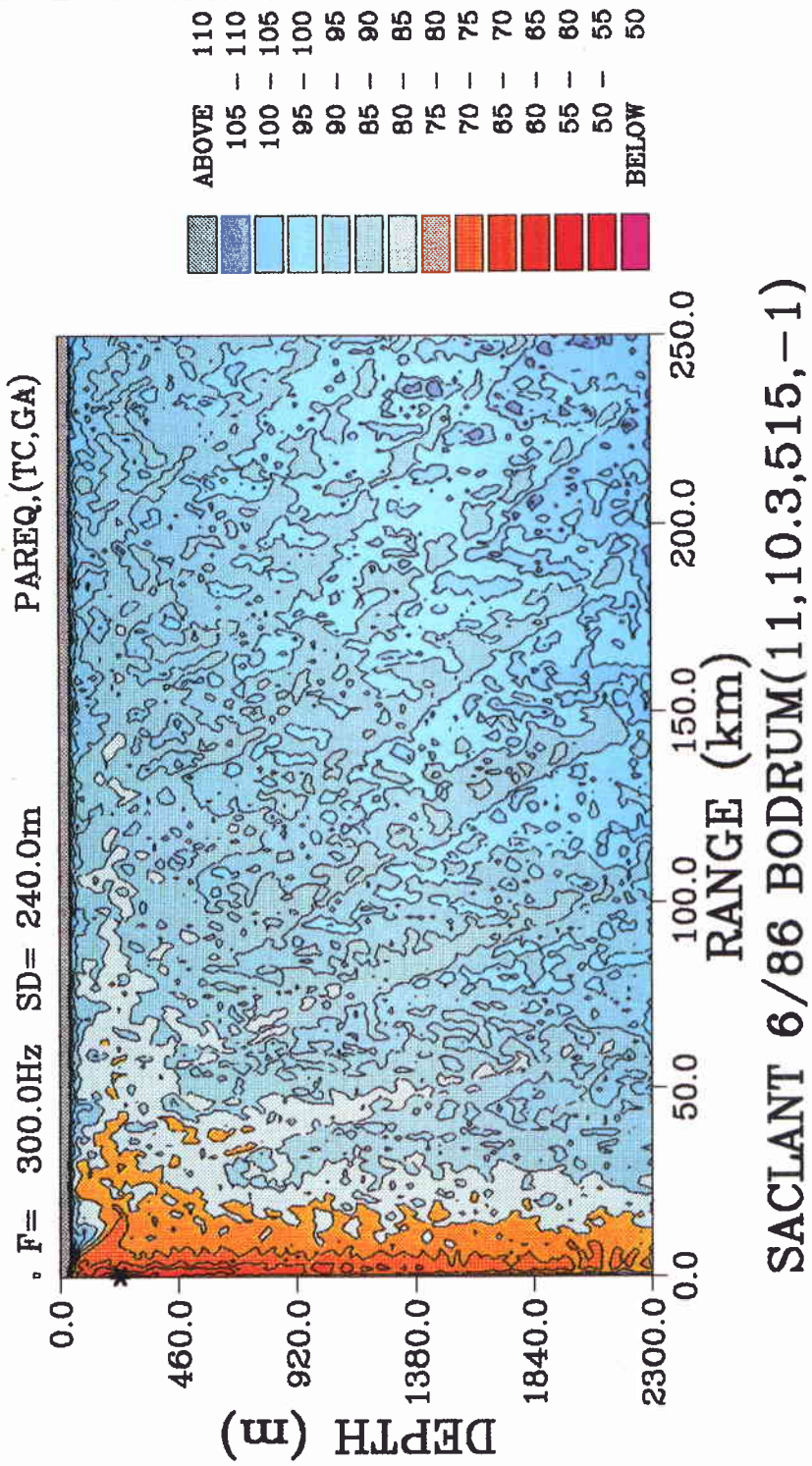

Figure A5 *Contour plot at 300 Hz, showing propagation loss intensity vs range and depth for a flat range segment.*

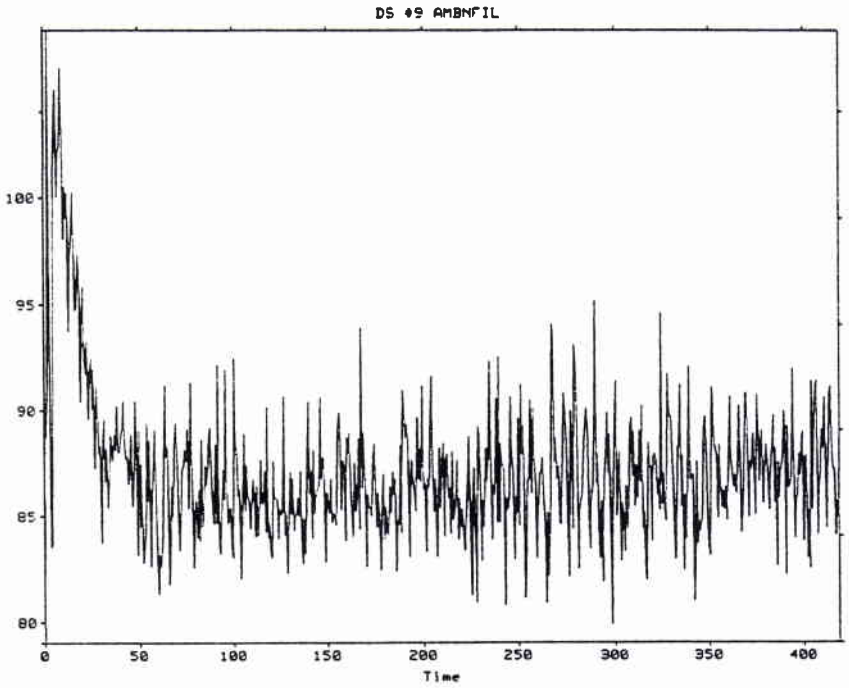

Figure A6 *Estimated omnidirectional noise-plus-reverberation spectrum levels as a function of time at 100 Hz during event 10; 32-hydrophone average.*

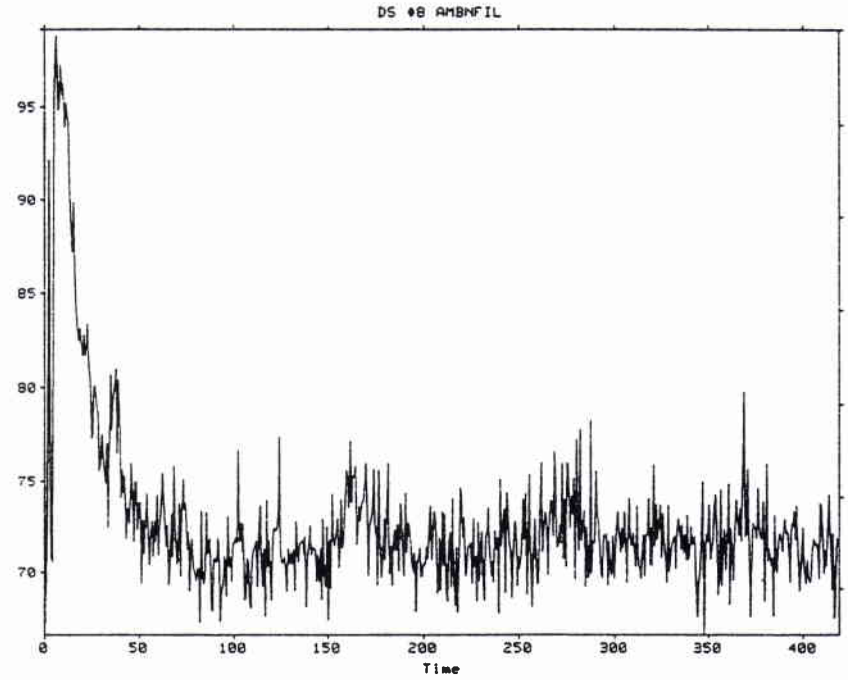

Figure A7 *Estimated omnidirectional noise-plus-reverberation spectrum levels as a function of time at 300 Hz during event 10; 32-hydrophone average.*

Ambient noise The Levantine basin is characterized by dense shipping and the observed sea-state for the experiment was $\sim$ 2–3.

Figures A6 and A7 show the measured estimate of omnidirectional noise-plus-reverberation *vs* time at 100 and 300 Hz, respectively. These estimates are derived from power spectra density measurements that were taken in a FFT bin with a width of 1.46 Hz, corrected to 1 Hz and averaged over all 32 hydrophones of the towed array. These data have been taken from event 2. The pre-shot omnidirectional noise estimates from the data in the above manner are probably due mainly to the towed-array self noise and towship and are given by:

Freq. (Hz)	Level (dB//1μPa/$\sqrt{}$ Hz)
100	88
300	72
450	68
730	65

Appendix B

Data processing description

A frequency domain beamformer derived from earlier work in explosives-induced reverberation [1] was the starting point for data processing in this work. It requires a two-dimensional fast fourier transform (FFT) of the array data which has been sampled in space and time and the averaging of the data over a selected frequency band. For each block of input data, an output block is generated, giving received acoustic power *vs* look direction at one center frequency. Each successive data block results in a similar output for the next time interval. This beamforming process, used for both the towed and vertical array, must be repeated for each desired center frequency.

To execute this process, a 512-point time domain FFT is applied to all 32 channels after Hann weighting is applied in the time domain. This results in 32 sets of 512 complex frequency domain samples – one set per hydrophone. A 50 Hz band of frequency bins about the desired output center frequency is selected for making a frequency averaged power estimate. For each frequency bin in the selected band, another Hann window is applied, the 32 spatial samples are zero padded out to 128 complex samples, and a 128-point space to wavenumber FFT is performed on the spatial samples. This results in a complex frequency *vs* wavenumber matrix of Fourier coefficients.

At the sampling frequency of 750 Hz used for the 100 and 300 Hz processing, the frequency resolution is $750/512 = 1.46$ Hz. The 50 Hz band average requires ca. 34 frequency bins to be used. These 34 bins by 128 wavenumbers are used to get an averaged received beam power *vs* wavenumber on the array. If the output desired is power *vs* angle, then because wavenumber is a linear function of frequency, an angle averaged power at the desired frequency involves averaging over a sloped line in frequency-wavenumber space according to a procedure described in [1,2]. This procedure is repeated for up to 1024 time epochs, depending on data length. The data are then presented in the form of beam power plots that show beam power spectrum levels *vs* time for angles from $-90°$ to $+90°$ relative to array broadside, with $+90°$ being the forward endfire direction for the towed array and directed at the surface for the vertical array. For the low-frequency data, the data block length is $512/750$ (or ~ 0.67 s).

Initial Distribution for SM-226

Ministries of Defence	
JSPHQ Belgium	2
DND Canada	10
CHOD Denmark	8
MOD France	8
MOD Germany	15
MOD Greece	11
MOD Italy	10
MOD Netherlands	12
CHOD Norway	10
MOD Portugal	5
MOD Spain	2
MOD Turkey	5
MOD UK	20
SECDEF US	60

NATO Authorities	
Defence Planning Committee	3
NAMILCOM	2
SACLANT	3
CINCIBERLANT	1

SCNR for SACLANTCEN	
SCNR Belgium	1
SCNR Canada	1
SCNR Denmark	1
SCNR Germany	1
SCNR Greece	1
SCNR Italy	1
SCNR Netherlands	1
SCNR Norway	1
SCNR Portugal	1
SCNR Spain	1
SCNR Turkey	1
SCNR UK	1
SCNR US	2
SECGEN Rep. SCNR	1
NAMILCOM Rep. SCNR	1

National Liaison Officers	
NLO Canada	1
NLO Denmark	1
NLO Germany	1
NLO Italy	1
NLO Netherlands	1
NLO UK	1
NLO US	1

NLR to SACLANT	
NLR Belgium	1
NLR Canada	1
NLR Denmark	1
NLR Germany	1
NLR Greece	1
NLR Italy	1
NLR Netherlands	1
NLR Norway	1
NLR Portugal	1
NLR Turkey	1
NLR UK	1

Total external distribution	221
SACLANTCEN Library	10
Stock	29
Total number of copies	260